

Momentum distribution of a Fermi gas of atoms in the BCS-BEC crossover

C. A. Regal^{1,*}, M. Greiner¹, S. Giorgini^{1,2}, M. Holland¹, and D. S. Jin^{1†}
¹*JILA, National Institute of Standards and Technology and University of Colorado,
and Department of Physics, University of Colorado, Boulder, CO 80309-0440, USA*
²*Dipartimento di Fisica, Università di Trento and BEC-INFN, I-38050 Povo, Italy*
(Dated: May 1, 2019)

We observe dramatic changes in the atomic momentum distribution of a Fermi gas in the region of the BCS-BEC crossover. We study the shape of the momentum distribution and the kinetic energy as a function of interaction strength. The momentum distributions are compared to a mean-field crossover theory, and the kinetic energy is compared to theories for the two weakly interacting limits. The temperature dependence of the distribution is also presented.

Recent years have seen the emergence of an intriguing Fermi system achieved with ultracold gases of ⁴⁰K or ⁶Li atoms. With these systems it is possible to widely tune the interatomic interaction strength, represented dimensionlessly as $k_F a$, where k_F is the Fermi wavevector and a is the scattering length. Of particular interest is the strongly interacting regime ($-1 < 1/k_F a < 1$) where a crossover between BCS theory of superconductivity and Bose-Einstein condensation (BEC) of molecules occurs [1, 2, 3]. Experiments have shown that these Fermi systems cross a phase transition as a function of temperature and display features of the BCS-BEC crossover such as a pairing gap, Δ , on order of the Fermi energy, E_F . Experimental probes have been numerous and include studies of molecule formation [4, 5, 6, 7, 8], thermodynamic properties [9, 10, 11, 12, 13, 14], condensate formation in the crossover [15, 16], collective excitations [17, 18], single-particle excitations [19, 20], and vortices [21].

One classic phenomenon associated with pairing in a Fermi system that has yet to be explored fully in atomic systems is a broadening of the Fermi surface in momentum space (see for example [22]). Figure 1 (inset) shows the expected momentum distribution of a homogeneous, zero temperature ($T = 0$) Fermi system. In the BCS limit ($1/k_F a \rightarrow -\infty$) the amount of broadening is small and associated with Δ . As the interaction increases this effect grows until at unitarity ($1/k_F a = 0$) the effect is on order of E_F , and in the BEC limit ($1/k_F a \rightarrow \infty$) the momentum distribution becomes the square of the Fourier transform of the molecule wavefunction.

In this Letter we present a measurement of the atom momentum distribution of a trapped Fermi gas in the BCS-BEC crossover regime. To perform these experiments we prepare a ⁴⁰K gas near a scattering resonance known as a Feshbach resonance, where we can tune the s-wave interaction between fermions by varying the magnetic field B [10, 23]. To probe the system we use the standard technique of time-of-flight expansion followed by absorption imaging [24]. To measure the momentum distribution of atoms the gas must expand freely without any interatomic interactions; to achieve this we quickly change the scattering length to zero for the expansion. Bourdel *et al.* pioneered this type of measurement using

a gas of ⁶Li atoms at $T/T_F \approx 0.6$, where T_F is the Fermi temperature [11]. Here we report measurements down to $T/T_F \approx 0.1$, where pairing becomes a significant effect and condensates have been observed [15, 16].

To understand what we expect for our trapped atomic system, we can predict the atomic momentum distribution using a local density approximation and the results for the homogeneous case. In the trapped gas case, in addition to the local broadening of the momentum distribution due to pairing, attractive interactions compress the density profile and thereby enlarge the overall momentum distribution. Figure 1 shows an integrated column density from the result of a mean-field calculation at $T = 0$ as described in Ref. [25] [26].

In our experimental setup we create an ultracold ⁴⁰K gas using previously described cooling techniques [10, 27]. The gas is prepared in a nearly equal mixture of the spin-states $|f, m_f\rangle = |9/2, -9/2\rangle$ and $|9/2, -7/2\rangle$, where f is the total spin and m_f the spin-projection quantum number. The final ultracold gas is held in an optical dipole trap formed at the intersection of two gaussian laser beams. One beam is oriented parallel to the force of gravity (\hat{y}) with a waist of $w_y = 200 \mu\text{m}$ and the second beam is perpendicular to the first (\hat{z}) and has $w_z = 15 \mu\text{m}$.

We first measured the atomic momentum distribution with our lowest temperature Fermi gas. We start with a weakly interacting gas at $T \approx 0.12 T_F$ in a trap with a radial frequency of $\nu_r = 280 \text{ Hz}$ and an aspect ratio of $\nu_z/\nu_r = 0.071$. We then adiabatically increase the interaction strength by ramping the magnetic field at a rate of $(6.5 \text{ ms/G})^{-1}$ to near a Feshbach resonance located at $202.10 \pm 0.07 \text{ G}$ [15]. After a delay of 1 ms, both dipole trap beams are switched off and simultaneously a magnetic-field ramp to $a \approx 0$ ($B = 209.6 \text{ G}$) at a rate of $(2 \mu\text{s/G})^{-1}$ is initiated. The rate of this magnetic-field ramp is designed to be fast compared to typical many-body timescales as determined by $\frac{\hbar}{E_F} = 90 \mu\text{s}$. The cloud is allowed to freely expand for 12.2 ms, and then an absorption image is taken. The imaging beam propagates along \hat{z} and selectively probes the $|9/2, -9/2\rangle$ state [10].

Samples of these absorption images, azimuthally averaged, are shown in Fig. 2 for various values of $1/k_F^0 a$, where the superscript 0 indicates a quantity that was

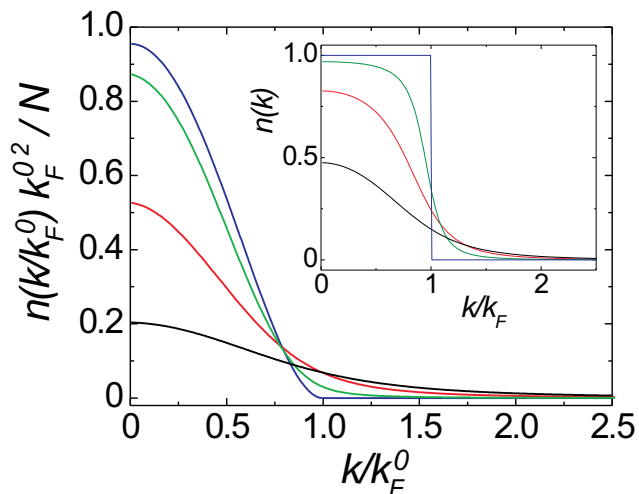


FIG. 1: (color online) Theoretical column integrated momentum distributions of a trapped Fermi gas $n(k)$ calculated from a mean-field theory [25]. N is the total particle number, k_F^0 is the non-interacting Fermi wavevector. The normalization is given by $2\pi \int n(k)kdk = N$, and we note that the normalization is strongly affected by the tail of the distribution. The lines correspond to $a = 0$ (blue), $1/k_F^0 a = -0.66$ (green), $1/k_F^0 a = 0$ (red), and $1/k_F^0 a = 0.59$ (black). (inset) Corresponding distributions for a homogeneous system.

measured in the weakly interacting regime. We observe a dramatic change in the distribution as predicted in Fig. 1. Some precautions need to be taken in quantitative comparison of Figs. 1 and 2. First, the magnetic-field ramp to the Feshbach resonance, while adiabatic with respect to most time scales, is not fully adiabatic with respect to the axial trap period. Second, in the experiment an adiabatic field ramp keeps the entropy of the gas, not T/T_F , constant. However, we expect the resulting change in T/T_F to have a minimal effect on the distribution for $1/k_F^0 a < 0$ [28]. Third, the theory assumes $T = 0$ and does not include the Hartree term, thus underestimating the broadening on the BCS side compared to a full theory [29].

It is natural now to consider extracting the kinetic energy from the momentum distribution. While the momentum distribution should be universal for small momenta, for large momenta it is influenced by details of the interatomic scattering potential. In the extreme case of a delta potential, which we used for the calculation in Fig. 1, the momentum distribution has a tail with a $1/k^4$ dependence, giving rise to a divergence of the kinetic energy. In the experiment we avoid a dependence of the measured kinetic energy on details of the interatomic potential because our magnetic-field ramp is never fast enough to access features on order of the interaction length of the Van der Waals potential, $r_0 \approx 60 a_0$ for ^{40}K [30]. Thus, the results presented in this Letter

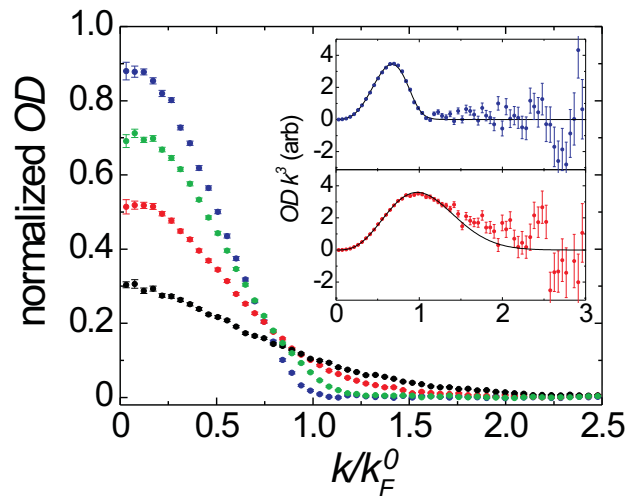


FIG. 2: (color online) Experimental, azimuthally averaged, momentum distributions of a trapped Fermi gas normalized such that the area under the curves is the same as in Fig. 1. The curves correspond to $1/k_F^0 a = -71$ (blue), -0.66 (green), 0 (red), and 0.59 (black). Error bars represent the standard deviation of the mean of averaged pixels. (inset) Curves for $1/k_F^0 a = -71$ (top) and 0 (bottom) weighted by k^3 . The lines are the results of a fit to Eqn. 1.

represent a universal quantity, independent of the details of the interatomic potential. Although universal in this sense, the measured kinetic energy is intrinsically dependent on the dynamics of the magnetic-field ramp, with faster ramps corresponding to higher measured energies.

To obtain the kinetic energy from the experimental data exactly we would need to take the second moment of the distribution, which is proportional to $\sum k^3 OD / \sum k OD$, where OD is the optical depth. As illustrated in Fig. 2 (inset) this is difficult due to the decreased signal-to-noise ratio for large k . Thus, our approach will be to apply a 2D surface fit to the image and extract an energy from the fitted function. In the limit of weak interactions the appropriate function is that for an ideal, harmonically trapped Fermi gas. This is

$$OD(x, y) = pk g_2(-\zeta e^{-\frac{x^2}{2\sigma_x^2} - \frac{y^2}{2\sigma_y^2}}) / g_2(-\zeta) \quad (1)$$

where $g_n(x) = \sum_{k=1}^{\infty} \frac{x^k}{k^n}$, ζ is the fugacity, $\sigma_{x,y}^2$ are proportional to the Fermi gas temperature, and pk is the maximum OD. Assuming isotropic expansion in all three dimensions the kinetic energy per particle is given by

$$E_{kin} = \frac{3 m \sigma_x \sigma_y}{2 t^2} \frac{g_4(-\zeta)}{g_3(-\zeta)} \quad (2)$$

where m is the mass of ^{40}K and t is the expansion time. Empirically, we find Eqn. 1 fits reasonably well to data throughout the crossover, as illustrated in Fig. 2 (inset).

Figure 3 shows the result of extracting E_{kin} as a function of $1/k_F^0 a$; we see that E_{kin} more than doubles between the non-interacting regime and unitarity. We have checked that heating and loss due to inelastic processes are negligible up to $1/k_F a \sim 0$. To do this we performed an experiment in which we adiabatically approach the Feshbach resonance at rate of $(6 \text{ ms/G})^{-1}$, wait 1 ms, and then ramp back at the same slow rate to the weakly interacting regime. If we start with a cloud initially at $T/T_F = 0.10$, T/T_F upon return increases by less than 10% for a ramp to $1/k_F a = 0$ (yet by 80% for a ramp to $1/k_F^0 a = 0.5$).

Using the fitting function of Eqn. 1 we can also extract information about the shape of the distribution through the parameter ζ . Since ζ can range from -1 to ∞ it is convenient to plot the quantity $\ln(1 + \zeta)$ (Fig. 4). We find that the shape evolves smoothly from that of an ideal Fermi gas at $T/T_F \sim 0.1$ in the weakly interacting regime, to a gaussian near unitarity, and to a shape more peaked than a gaussian in the BEC regime. These qualitative features are predicted by the mean-field calculation of the distributions in Fig. 1.

As mentioned earlier E_{kin} of a trapped gas is affected both by the broadening due to pairing (Fig. 1 (inset)) and by changes in the trapped gas density profile. In the BCS limit, the broadening due to pairing scales with $e^{-\pi/2k_F|a|}$ and is thus exponentially small compared to density profile changes, which scale linearly with $k_F|a|$. In this limit we can calculate E_{kin}/E_{kin}^0 using a mean-field calculation in the normal state [31] to find, to lowest order in $k_F^0|a|$, $E_{kin}/E_{kin}^0 = \frac{2048}{945\pi^2} k_F^0|a| + 1$. We plot this result in Fig. 3 (inset) and find good agreement for the weakly interacting regime ($1/k_F^0|a| > 1$). In the crossover regime where the pairs are more tightly bound, pairing provides a significant contribution to the change in the momentum distribution. At unitarity a full Monte Carlo calculation predicts the radius of the Fermi gas density profile to become $(1 + \beta)^{1/4} R_0 = 0.81 R_0$, where R_0 is the Thomas-Fermi radius of a non-interacting Fermi gas [29]. Just this rescaling would result in $E_{kin}/E_{kin}^0 = 1.54$ (green bar in Fig. 3). Thus, at unitarity, pairing effects on the momentum distribution must account for a large fraction of the measured value of $E_{kin}/E_{kin}^0 = 2.3 \pm 0.3$ (Fig. 3) and all of the observed change in distribution shape (Fig. 4).

In the BEC limit we expect the measured energy to be that of an isolated diatomic molecule after dissociation by the magnetic-field ramp. Provided the scattering length associated with the initial molecular state, $a(t=0)$, is much larger than $r_0 \approx 60 a_0$, the wave function for the molecule is given by $\psi = e^{-r/a(t=0)}/r$ where r is the internuclear separation. We can calculate the measured energy from the solution of the Schrödinger equation with a time-dependent boundary condition on the two-particle wavefunction $\left. \frac{d \log(r\psi)}{dr} \right|_{r=0} = -\frac{1}{a(t)}$, where

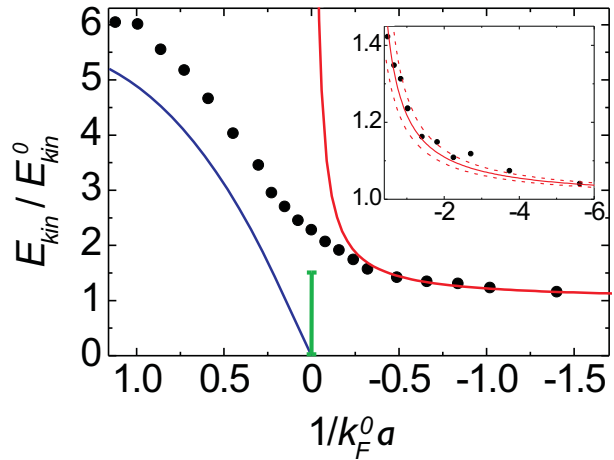


FIG. 3: (color online) The points (\bullet) show the measured energy E_{kin} normalized to $E_{kin}^0 = 0.25 k_b \mu\text{K}$ ($E_{kin}^0 = \frac{3}{8} E_F$ for a harmonically trapped gas at $T = 0$). The red line is the expected energy ratio from a calculation only valid in the weakly interacting regime ($1/k_F a < -1$). In the strongly interacting regime pairing due to many-body effects strongly increases E_{kin} . The green bar represents the expected value of E_{kin}/E_{kin}^0 at unitarity just due to density profile rescaling (see text). In the molecule limit ($1/k_F^0 a > 1$) we calculate the expected energy for an isolated molecule (blue line). (inset) A focus on the weakly interacting regime with the same axes definitions as the main graph. The dashed lines show the uncertainty in the calculation based upon the uncertainty in the Feshbach resonance parameters [15, 23].

$a(t)$ is the scattering length fixed by the magnetic field at time t . In Fig. 3 we show the result of this calculation for a pure gas of molecules and a $(2 \mu\text{s/G})^{-1}$ ramp rate. We find reasonable agreement considering that there is a large systematic uncertainty in the theory curve due to the experimental uncertainty in the magnetic-field ramp rate and that this two-body theory should match the data only in the BEC limit ($1/k_F a \gg 1$).

We have also studied the dependence of the momentum distribution on $(T/T_F)^0$. To vary the temperature of our gas, we recompress the optical dipole trap after evaporation and parametrically heat the cloud [8]. The experimental sequence for measuring the momentum distribution is the same as above except the ramp rate to $a = 0$ for expansion was $\sim (8 \mu\text{s/G})^{-1}$. Figure 5 shows the measured kinetic energy change $\Delta E_{kin} = E_{kin} - E_{kin}^0$. On the BEC side of the resonance ($1/k_F a > 0$), ΔE_{kin} decreases dramatically with $(T/T_F)^0$. Because ΔE_{kin} should be proportional to the molecule fraction, this result is closely related to the recent observation that the molecule conversion efficiency scales with T/T_F [8]. In the strongly interacting regime we also observe a decrease in ΔE_{kin} with increasing $(T/T_F)^0$. Here the temperature dependence of ΔE_{kin} is consistent with the expectation

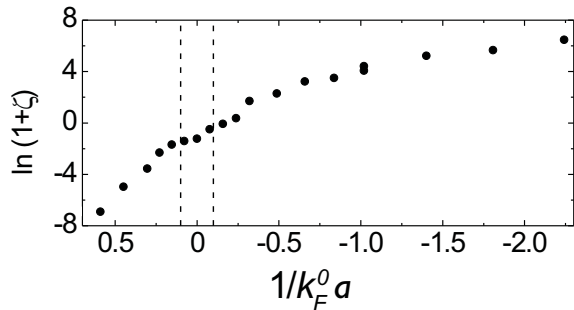


FIG. 4: Shape of the momentum distribution as described through the parameter ζ (Eqn. 1). $\ln(1 + \zeta) = 0$ corresponds to a gaussian distribution, and for an ideal Fermi gas $\ln(1 + \zeta)^{-1} \approx T/T_F$ in the limit of low T/T_F . The dashed lines show the uncertainty in the Feshbach resonance position [15].

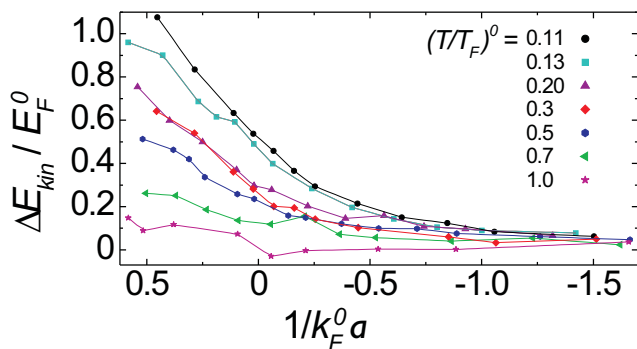


FIG. 5: (color online) Temperature dependence of $\Delta E_{kin} = E_{kin} - E_{kin}^0$ normalized to the Fermi energy at $a = 0$. $(T/T_F)^0$ is the temperature of the non-interacting gas [33]. For the coldest dataset (black) the peak density, for atoms in one of the two spin states, in the weakly interacting regime is $n_{pk}^0 = 1.4 \times 10^{13} \text{ cm}^{-3}$ and $E_F^0 = 0.56 \text{ } \mu\text{K}$. For the hottest dataset (magenta) n_{pk}^0 decreases to $6 \times 10^{12} \text{ cm}^{-3}$ and $E_F^0 = 0.79 \text{ } \mu\text{K}$.

that the changes in the kinetic energy are caused by pairing and not coherence [15, 19, 32].

We have found that the momentum distribution of a Fermi gas provides a wealth of information on crossover physics. The measurement is a probe of pairing in the strongly interacting regime, and it provides a universal thermodynamic quantity that is complementary to previously measured energies in the BCS-BEC crossover [9, 10, 11, 12, 13]. This work also provides a starting point for future experiments seeking to probe pair correlations in the momentum distribution using measurements of atom shot noise [34].

We thank Q. Chen and K. Levin for valuable discussions and J. T. Stewart for experimental assistance. This work was supported by NSF, NIST, and NASA. C. A. R. acknowledges support from the Hertz Foundation.

[†] Quantum Physics Division, National Institute of Standards and Technology.

- [1] M. Randeria, in *Bose-Einstein Condensation*, edited by A. Griffin, D. W. Snoke, and S. Stringari (Cambridge University, Cambridge, 1995), pp. 355–392, and references therein.
- [2] E. Timmermans, K. Furuya, P. W. Milonni, and A. K. Kerman, *Phys. Lett. A* **285**, 228 (2001).
- [3] M. Holland, S. J. J. M. F. Kokkelmans, M. L. Chiofalo, and R. Walser, *Phys. Rev. Lett.* **87**, 120406 (2001).
- [4] C. A. Regal, C. Ticknor, J. L. Bohn, and D. S. Jin, *Nature* **424**, 47 (2003).
- [5] K. E. Strecker, G. B. Partridge, and R. G. Hulet, *Phys. Rev. Lett.* **91**, 080406 (2003).
- [6] J. Cubizolles *et al.*, *Phys. Rev. Lett.* **91**, 240401 (2003).
- [7] S. Jochim *et al.*, *Phys. Rev. Lett.* **91**, 240402 (2003).
- [8] E. Hodby *et al.*, *Phys. Rev. Lett.* **94**, 120402 (2005).
- [9] K. M. O’Hara *et al.*, *Science* **298**, 2179 (2002).
- [10] C. A. Regal and D. S. Jin, *Phys. Rev. Lett.* **90**, 230404 (2003).
- [11] T. Bourdel *et al.*, *Phys. Rev. Lett.* **91**, 020402 (2003).
- [12] T. Bourdel *et al.*, *Phys. Rev. Lett.* **93**, 050401 (2004).
- [13] M. Bartenstein *et al.*, *Phys. Rev. Lett.* **92**, 120401 (2004).
- [14] J. Kinast *et al.*, *Science* **307**, 1296 (2005).
- [15] C. A. Regal, M. Greiner, and D. S. Jin, *Phys. Rev. Lett.* **92**, 040403 (2004).
- [16] M. Zwierlein *et al.*, *Phys. Rev. Lett.* **92**, 120403 (2004).
- [17] J. Kinast *et al.*, *Phys. Rev. Lett.* **92**, 150402 (2004).
- [18] M. Bartenstein *et al.*, *Phys. Rev. Lett.* **92**, 203201 (2004).
- [19] C. Chin *et al.*, *Science* **305**, 1128 (2004).
- [20] M. Greiner, C. A. Regal, and D. S. Jin, *Phys. Rev. Lett.* **94**, 070403 (2005).
- [21] M. Zwierlein *et al.*, *Nature* **435**, 1047 (2005).
- [22] P. G. de Gennes, *Superconductivity of Metals and Alloys* (Addison-Wesley, California, 1966).
- [23] C. A. Regal, C. Ticknor, J. L. Bohn, and D. S. Jin, *Phys. Rev. Lett.* **90**, 053201 (2003).
- [24] M. H. Anderson *et al.*, *Science* **269**, 198 (1995).
- [25] L. Viverit, S. Giorgini, L. Pitaevskii, and S. Stringari, *Phys. Rev. A* **69**, 013607 (2004).
- [26] A similar local density calculation at unitarity using the momentum distribution obtained from quantum Monte Carlo simulations shows good agreement with the mean-field result for this observable [29].
- [27] B. DeMarco and D. S. Jin, *Science* **285**, 1703 (1999).
- [28] Q. Chen, J. Stajic, and K. Levin, *cond-mat/0411090* (2005).
- [29] G. E. Astrakharchik *et al.*, *Phys. Rev. Lett.* **93**, 200404 (2004).
- [30] G. F. Gribakin and V. V. Flambaum, *Phys. Rev. A* **48**, 546 (1993).
- [31] L. Vichi and S. Stringari, *Phys. Rev. A* **60**, 4734 (1999).
- [32] Q. Chen, J. Stajic, S. Tan, and K. Levin, *Physics Reports* **412**, 1-88 (2005).
- [33] $(T/T_F)^0$ is measured by fitting to Eqn. 1 the momentum distributions measured near $a = 0$, probing along both \hat{x} and \hat{z} . Above $T/T_F = 0.45$ we fix ζ to zero and use a calculated correction factor to determine T/T_F .
- [34] M. Greiner, C. A. Regal, J. T. Stewart, and D. S. Jin, *Phys. Rev. Lett.* **94**, 110401 (2005).

* Email: regal@jilau1.colorado.edu